

# A 0.2-V Three-Winding Transformer-Based DCO in 16-nm FinFET CMOS

Chao-Chieh Li<sup>ID</sup>, Min-Shueh Yuan<sup>ID</sup>, *Member, IEEE*, Yu-Tso Lin, Chia-Chun Liao, Chih-Hsien Chang, *Member, IEEE*, and Robert Bogdan Staszewski<sup>ID</sup>, *Fellow, IEEE*

**Abstract**—In this brief, we introduce a 3.2–4 GHz three-winding transformer-based class-F digitally controlled oscillator (DCO) with a DC-DC booster for energy harvesting applications. A  $\pi$ -model is adopted for this multi-turn transformer to analyze its impedance transformation and overall loop gain. The trifilar coil generates large passive voltage loop gain, allowing the DCO supply voltage of 0.2 V to be even lower than the threshold voltage of transistors without any performance degradation. Due to the gate/drain isolation as well as smaller voltage-dependent capacitance in advanced FinFET technology, this brief achieves very low supply frequency pushing of 38 MHz/V. The switched capacitor placed at the tertiary winding can reach very fine resolution of 1.3 kHz due to the impedance transformations and source degeneration. The bias and control voltages of nearly zero power are generated with a switched-capacitor based DC-DC converter and a ring-based non-overlapped clock generator.

**Index Terms**—Digitally controlled oscillator (DCO), energy harvesting, transformer, trifilar, FinFET, DC converter, voltage booster.

## I. INTRODUCTION

**E**NERGY harvesting (EH) is a topic of intensive research, promising battery-free operation of massive networks of wireless IoT devices [1]. To fulfill that goal, IC circuits featuring ultra-low power (ULP) consumption with ultra-low voltage (ULV) supply are desired. As an example, thermal electric, human vibration and photovoltaic EH, as shown in Fig. 1, produce ULV supplies ( $<0.3$  V) that are well below the threshold voltage ( $V_{th}$ ) of even the most recent FinFET CMOS transistors, thus making it extremely challenging for circuit designers. On the other hand, all-digital PLLs (ADPLL) are well known for their friendliness to low supply voltages and immunity from supply perturbations [2]. The major part of

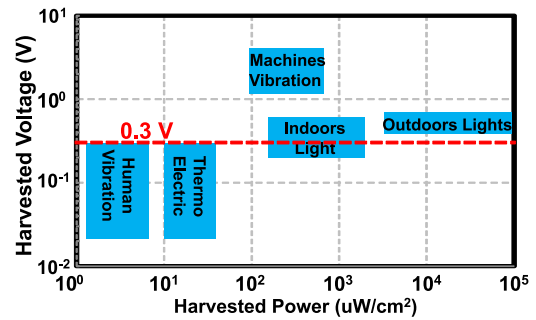


Fig. 1. Supply voltage from energy harvesters is typically low and highly dependent on the underlying energy activity.

power consumption in the whole ADPLL lies in a digitally controlled oscillator (DCO) [2], [3]. Thus, new special circuit techniques are needed to make the IoT devices function properly with supplies below  $V_{th}$ .

A transformer feedback oscillator [4] is a promising topology for ULV operation due to its passive RF voltage gain. However, the gates and drains of the cross-coupled transistors there share the same dc voltage. This causes the resonating frequency, mainly due to its voltage-dependent gate capacitance  $C_g$ , to strongly track (i.e., be pushed by) the supply voltage,  $V_{DD}$ . For EH, the supply pushing must be very low due to the significant temporal variability of harvested voltage, as indicated in Fig. 1. The varying harvested voltage could be hundreds of mV, which is  $>10\times$  larger than in conventional consumer IC designs.

A class-F oscillator [5] also provides a passive voltage gain, but the gates are electrically separated from the drains via the transformer, thus resulting in a low frequency pushing. However, its  $V_{DD}$  cannot readily go below  $V_{th}$  since the DCO tuning word voltage would not be able to reliably switch the capacitors at such low supply. In [6], a self voltage-boosting technique was proposed to provide a high-enough control voltage of VCO for the sufficient tuning range. A voltage booster using a GHz-level clock consumes excessive power and brings high frequency spurs, which must be then properly filtered.

This brief is an extension of our conference paper [7] in which a trifilar-coil oscillator topology providing large passive voltage gain was proposed to enable the sub- $V_{th}$  operation. A  $\pi$ -model for a three-winding transformer is introduced to explain the resonant frequency and impedance transformation which helps to generate fine tune resolution. The source of the oscillator transistor is not tied to ground, hence the gate-source

Manuscript received January 11, 2020; revised March 23, 2020; accepted April 14, 2020. Date of publication April 21, 2020; date of current version November 24, 2020. This work was supported in part by the Science Foundation Ireland under Grant 14/RP/I2921. This brief was recommended by Associate Editor L. A. B. G. Oliveira. (*Corresponding author: Chao-Chieh Li.*)

Chao-Chieh Li is with the Mixed-Signal Design Department, Taiwan Semiconductor Manufacturing Company, Hsinchu 300-77, Taiwan, and also with the School of Electrical and Electronic Engineering, University College Dublin, Dublin D04, Ireland (e-mail: jlliv@tsmc.com).

Min-Shueh Yuan, Yu-Tso Lin, Chia-Chun Liao, and Chih-Hsien Chang are with the Mixed-Signal Design Department, Taiwan Semiconductor Manufacturing Company, Hsinchu 300-77, Taiwan.

Robert Bogdan Staszewski is with the School of Electrical and Electronic Engineering, University College Dublin, Dublin D04, Ireland (e-mail: robert.staszewski@ucd.ie).

Color versions of one or more of the figures in this article are available online at <https://ieeexplore.ieee.org>.

Digital Object Identifier 10.1109/TCSII.2020.2989415

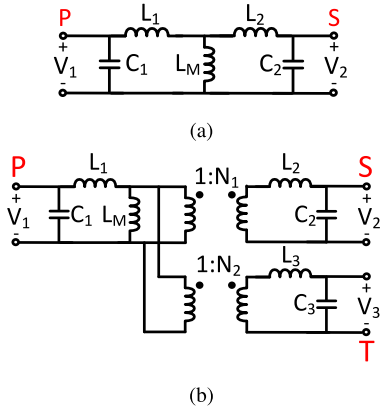


Fig. 2. (a) T-model for a 2-winding transformer-based resonator. (b)  $\pi$ -model for a 3-winding transformer-based resonator.

( $V_{GS}$ ) swing can be larger than in the conventional common-source cross-coupled pair topology. The 3rd-harmonic tone is coupled from the primary resonator to the source side, making a smaller effective ISF function. Due to the gate/drain isolation as well as smaller voltage dependent-capacitance in advanced FinFET technology, this brief achieves very low frequency pushing. To provide the bias and control voltages which are higher than  $V_{DD}$ , a switched-capacitor based DC-DC converter with a ring-based non-overlapped clock generator is proposed featuring a nearly zero power consumption.

## II. THREE-WINDING RESONATOR DESIGN

A conventional *two*-winding 1:2 transformer in a class-F oscillator can be thoroughly analyzed by a T-model of Fig. 2(a) [5]. However, if the number of windings is larger than 2, it is hard to adopt the T-model due to the duplicate mutual inductance effects. In [8], a  $\pi$ -model was adopted for a *multi*-winding transformer. In Fig. 2(b),  $V_1$ ,  $V_2$  and  $V_3$  represent the primary, secondary and tertiary voltage sources. There are two ideal transformers in the middle with a perfect coupling coefficient  $k = 1$ . Capacitors  $C_1$ ,  $C_2$  and  $C_3$  are digitally tunable to control the resonant characteristic of the network. The values of various inductances and turns ratios are captured in formulas (1)–(3) [8]:

$$N_1 = \frac{L_{M23}}{L_{M13}}, N_2 = \frac{L_{M23}}{L_{M12}} \quad (1)$$

$$L_M = \frac{L_{M12}L_{M13}}{L_{M23}}, L_1 = L_{11} - \frac{L_{M12}L_{M13}}{L_{M23}} \quad (2)$$

$$L_2 = L_{22} - \frac{L_{M12}L_{M23}}{L_{M13}}, L_3 = L_{33} - \frac{L_{M23}L_{M13}}{L_{M12}} \quad (3)$$

where  $L_{11}$ ,  $L_{22}$  and  $L_{33}$  represent self-inductances of the primary, secondary and tertiary coils, respectively. Inductance  $L_1$  equals  $L_{11}$  minus  $L_M$ , which is a mutual inductance part. Without the magnetic coupling,  $L_1$  reduces to the self-inductance  $L_{11}$ . Terms  $L_{M12}$ ,  $L_{M23}$  and  $L_{M13}$  represent mutual inductances between  $L_{11}$ ,  $L_{22}$  and  $L_{33}$ , which could be obtained from electromagnetic (EM) simulations or measured with the other windings unloaded. From Fig. 2(b), the impedance transformation could be easily realized by the ideal

transformers 1: $N_1$  and 1: $N_2$ . To calculate the equivalent inductance ( $L_{eq}$ ) seen from the primary coil, capacitors  $C_{1-3}$  are expediently removed. In this design, the secondary coil is connected to a high impedance (MOS gate), so the end-point of  $L_2$  is considered open and its inductance could be ignored. Then,  $L_{eq}$  could be obtained as:

$$L_{eq} = \frac{N_2^2 L_1 L_M + L_1 L_3 + L_M L_3}{L_M N_2^2 + L_3} \quad (4)$$

The equivalent capacitance seen from the primary coil could be also derived from the impedance transformations:

$$C_{eq} = C_1 + N_1^2 C_2 + N_2^2 C_3 \quad (5)$$

In this design,  $N_1$  and  $N_2$  are equal to 1.87 and 0.37, respectively. Hence,  $N_2^2$  is significantly smaller than 1 and so  $C_3$  could be neglected in  $C_{eq}$ . Thus, the resonant frequency seen from the primary coil is derived as:

$$\omega_{osc} = \sqrt{\frac{1}{(C_1 + N_1^2 C_2) \frac{N_2^2 L_1 L_M + L_1 L_3 + L_M L_3}{L_M N_2^2 + L_3}}} \quad (6)$$

$L_M$ ,  $L_1$ ,  $L_2$  and  $L_3$  are equal to 0.41, 0.15, 0.29 and 0.37 nH, respectively.  $C_1$  and  $C_2$  are set to 1 pF. The estimated resonant frequency is 3.34 GHz which is within a 3% error from EM simulations. Since the DCO requires a variable capacitance for frequency tuning, the DCO gain ( $K_{DCO}$ ) could be derived as [2]:

$$K_{DCO}(f) = 2\pi^2 (L_{eq} \cdot \Delta C) f^3 \quad (7)$$

$K_{DCO}(f)$  is a frequency step in response to a small digitally induced  $\Delta C$  step. If  $\Delta C$  is placed at the tertiary coil,  $K_{DCO}$  could be re-written as:

$$K_{DCO,T}(f) = 2\pi^2 [L_{eq} \cdot \left( \frac{N_2^2}{1 + N_1^2 + N_2^2} \right) \cdot \Delta C_3] f^3 \quad (8)$$

$K_{DCO,T}$  represents the DCO gain contributed by the tertiary resonator. Eq. (8) shows that  $\Delta C_3$  will experience a  $0.03\times$  reduction. This helps with generating very fine tuning resolution (i.e., low  $K_{DCO}$ ) by setting a small ratio of  $N_2^2/(1 + N_1^2 + N_2^2)$ . The very fine  $K_{DCO}$  helps with reducing the quantization noise of ADPLL in order to avoid a power hungry  $\Sigma\Delta$  modulator [2], [9].

To leverage the advantage of class-F operation from a significant presence of the 3rd harmonic, the turns ratio of primary to secondary is set to 1:2 in this design. In Fig. 3,  $Z_{in}$  into the primary represents the input impedance seen from  $V_1$  with a 3rd harmonic tone. By setting  $C_1 = C_2 = C_3$ ,  $Z_{in}$  of the tertiary could also have a strong 3rd harmonic impedance peaking as shown by the blue curve. If the tertiary winding is adopted at the source side of MOS,  $V_{GS}$  could be reshaped to benefit from the lowered impulse sensitivity function (ISF).

## III. DESIGN OF TRIFILAR DCO

The conventional class-F oscillator can provide a nearly  $2\times$  passive voltage gain due to the 1:2 turns-ratio transformer from the drain (D) to gate (G) of the MOS transistors. In the proposed trifilar oscillator, the passive voltage gain is *enhanced* by another winding located at the source (S) of the cross-coupled transistors, as shown in Fig. 4(a). The tertiary

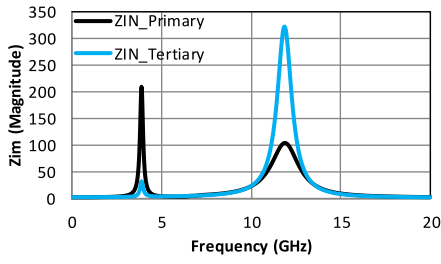


Fig. 3. Input impedances of three-winding transformer tank.

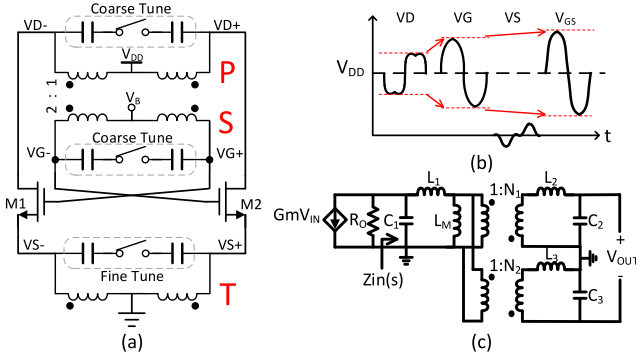


Fig. 4. Proposed trifilar oscillator: (a) schematic, (b) time-domain waveforms, (c) small signal  $\pi$ -model.

winding is coupled through a weak magnetic coupling  $1:N_2$  from the original primary winding. Consequently, the NMOS source signal ( $V_S$ ) oscillates around the ground dc level and produces a voltage swing in the opposite direction to that of  $V_G$ , thus enhancing  $V_{GS}$ , as shown in Fig. 4(b). A higher effective  $V_{GS}$  is thus achieved.

Voltage  $V_B$  controls the gate bias of cross-coupled NMOS independently from  $V_{DD}$  due to the isolating effect of the transformer. The nonlinear capacitance  $C_G$  is typically  $3\times$  larger than  $C_D$  and so it would normally be the main contributor to the frequency pushing. Since  $V_B$  does not drain any current, it can undergo a heavy low-pass filtering to eliminate any of its transient effects on  $C_G$ .

The coarse bank with 23 MHz/bit is split between the transformer's primary and secondary windings to achieve the maximum Q enhancement [5]. The switched-capacitor at the source side can reach a very fine resolution of 1.3 kHz, as suggested by (8), which could help in eliminating the power-hungry  $\Sigma\Delta$  modulator in an ADPLL.

The small-signal model of the trifilar oscillator is shown in Fig. 4(c). The primary side in Fig. 2(b) is equivalent to the drain side of cross-coupled MOS, and so on. The voltage loop gain could be derived by the formula for  $V_{out}/V_{in}$ :

$$\frac{V_{out}}{V_{in}} \simeq g_m(R_O || Z_{in}(s)) \frac{L_M}{L_{11}} (N_1 + N_2) \quad (10)$$

$Z_{in}(s)$  could be represented the long formula (9), as shown at the bottom of the page. From Eq. (10), the voltage loop gain

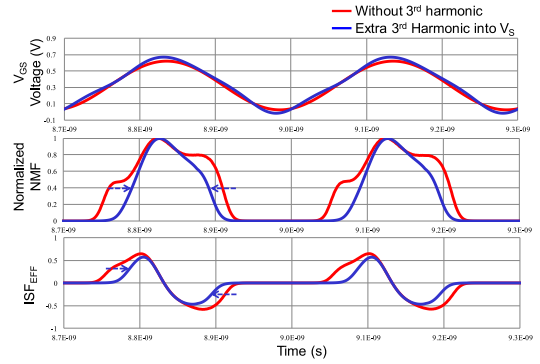


Fig. 5. ISF function benefiting from the 3<sup>rd</sup> harmonic injection.

could be enhanced by the term  $(N_1 + N_2)$ . For the same start-up condition, the device's required transconductance  $g_m$  could be reduced 55% at the sub- $V_{th}$  bias while the passive voltage gain is already boosted up by 220% [2]. Thus, the supply voltage could be brought down to 0.2 V or lower, while still ensuring the reliable oscillation start-up. As shown in Eq. (10), higher  $N_1$  and  $N_2$  beneficially bring higher passive voltage gain. However, excessively large  $N_2$  might bring strong source degeneration and degrade the MOS'  $g_m$ . In Fig. 4(c),  $G_m V_{in}$  and  $R_O$  bypass the tertiary winding for the sake of simplified derivation. The value of  $N_2$  needs to be traded off between the active and passive voltage gains.

For the three-winding transformer, the effective quality factor could be calculated by  $Q_{tri} = \Im(Z_{tot})/\Re(Z_{tot})$ . The total  $Q_{tri}$  will be a weighted combination of  $Q$ -factors of the three coils. Two thick metals and one ultra-thick metal are combined to achieve the lowest possible series resistance for the maximum  $Q$ -factor and minimum voltage drop in the supply path.  $Q_{tri}$  exceeds 11 within 3–4 GHz of the DCO tuning range (TR).

#### IV. PHASE NOISE (PN)

Figure 5 demonstrates the ISF function benefiting from the 3rd harmonic injection. At the top, the red curve is a waveform  $V_{GS}$  of the original class-F oscillator. The blue curves contain an additional 3rd harmonic injected into the source, thus achieving a higher amplitude by the tertiary feedback. At the zero-crossing points, the 3rd harmonic injection helps to narrow down the zero-crossing regions where the injected noise can severely degrade the phase noise. This effectively reduces the normalized noise modulating function (NMF) as indicated by the arrows at the middle of Fig. 5. Thus, a smaller effective ISF function and lower ( $\sim 2$  dB) PN could be achieved.

#### V. DC-TO-DC CONVERTER

As mentioned above, if the available supply is below  $V_{th}$ , then the sub-threshold control voltage of the switched-capacitor will lead to a very narrow tuning range. Furthermore, as this topology separates the drains and gates to enhance the overall  $g_m$  at low  $V_{DD}$ ,  $V_B$  bias higher than  $V_{DD}$  is needed

$$Z_{in}(s) = \frac{s(N_2^2 L_1 L_M + L_1 L_3 + L_M L_3)}{s^2(N_2^2 L_1 L_M + L_1 L_3 + L_M L_3)(C_1 + N_1^2 C_2) + L_M N_2^2 + L_3} \quad (9)$$

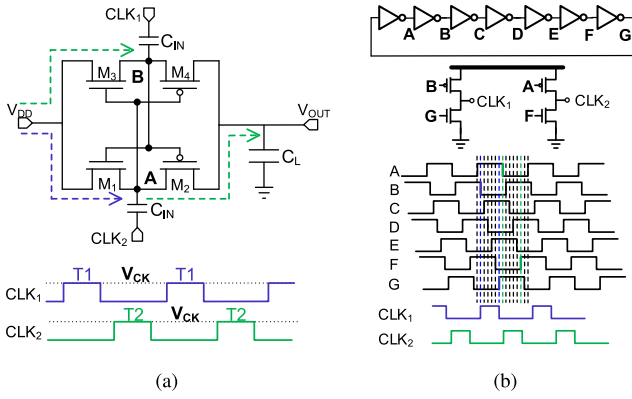


Fig. 6. (a) Voltage booster schematic. (b) Ring-based non-overlapped clock generator.

in the sub- $V_{th}$  operation. Consequently, a tiny DC-to-DC converter coupled to the harvested voltage is proposed to provide a nearly static control  $V_{ctrl}$  and bias  $V_B$  for the trifilar DCO. A cross-coupled voltage booster could help to generate  $V_{DD}+V_{CK}$  by the nonoverlapped clocks  $CLK_1$  and  $CLK_2$ , as shown in Fig. 6(a). During  $T_1$ , point A is charged to near  $V_{DD}$ . In the next interval,  $T_2$ ,  $CLK_2$  changes from 0 V to  $V_{DD}$  and point B is charged to near  $V_{DD}$  and waiting for the next period for the boost-up. The important concern is for  $CLK_1$  and  $CLK_2$  to be non-overlapped; otherwise,  $M_1$  and  $M_2$  might be turned-on simultaneously and degrade the level of  $V_{OUT}$ .  $C_{IN}$  is designed to ensure the adequate current sinking from  $V_{OUT}$ . In this design,  $V_B$  drains no static current due to the gate load connection and static control.  $V_{ctrl}$  only consumes drain/source leakage of the buffer which drives the frequency tuning switched-capacitor. Thus,  $C_{IN}$  could be at the level of only tens of fF.

In conventional designs, a non-overlapped clock generator often comprises combinatorial logic to generate certain delays. A logic cell (e.g., NAND, NOR) usually requires at least three stacked MOS transistors, thus raising the minimum operational level of  $V_{DD}$ . Here, a non-overlapped clock generator is proposed using a simple ring oscillator (RO) with a clock gating technique, as shown in Fig. 6(b). A multi-phase single-ended 7-stage RO generates seven clock phases, from A to G. The switcher's inverters use a different gate control to generate the rising/falling edges of  $CLK_1$  and  $CLK_2$ . Thus, the nonoverlapped period is defined as  $T_{RO}/N$ , where  $T_{RO}$  is the period of ring oscillator and  $N = 7$  is the number of RO stages. The number of series-connected MOS in this circuit will not exceed two, which helps to operate at  $V_{DD}$  lower than 0.2 V.  $V_{in}$  provides the input to the voltage booster and directly controls the drain side of MOS. To save extra power from the RO, the oscillation frequency is set to tens of MHz by using small W/L-ratio inverters.

## VI. CIRCUIT IMPLEMENTATION

Figure 7 presents the overall view of this design. Five voltage booster stages driven by the non-overlapped clock generator provide a sufficiently high voltage to turn on the switched capacitors. This way, the full tuning range (i.e., <20%) can be recovered. A high-enough voltage for  $V_{ctrl}$

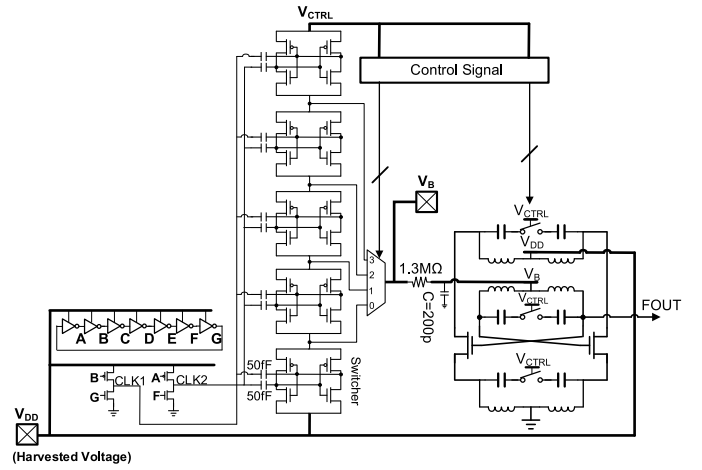


Fig. 7. Trifilar DCO with DC-DC converter.

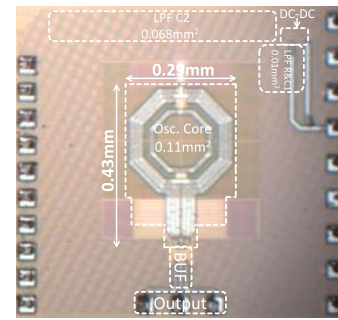


Fig. 8. Die micrograph.

could also help to eliminate the frequency pushing effect from these switches.  $V_B$  uses a selected voltage booster output. Low-pass filter of 3 kHz corner is adopted to eliminate the ripple from voltage booster and to prevent the DCO PN degradation. Ripples of the lower frequency (i.e., <30 kHz) could be mitigated by the eventual ADPLL loop.

## VII. MEASUREMENT

The proposed trifilar DCO is implemented in 16-nm FinFET CMOS, whose chip micrograph is shown in Fig. 8. Figure 9 shows on-wafer phase noise measurements. At the  $V_{DD} = 0.4$  V setting, phase noise (PN) reaches  $-120$  to  $-123$  dBc/Hz and  $-143$  to  $-145$  dBc/Hz at 1 MHz and 10 MHz offsets, respectively. FOM is 188–191 dBc/Hz with a power consumption of 3.8 mW. In the  $V_{DD} = 0.2$  V mode, the PN worsens to  $-111 \sim -113$  dBc/Hz and  $-132 \sim -135$  dBc/Hz at 1 MHz and 10 MHz offsets, respectively, but the power consumption reduces to 0.6 mW, yielding FOM of 186–188 dB. The flicker PN corner is 40 kHz and 120 kHz at 0.2 V and 0.4 V, respectively. The frequency pushing in Fig. 10(a)(b) shows a small value of 3.627 MHz/V at 0.4 V and 12.6–38.2 MHz/V at 0.2 V. The coarse step size is 23 MHz/bit and the fine step is 1.3 kHz/bit. The DC-to-DC converter could operate at as low as 0.15 V, consuming only 0.2  $\mu$ W at the 0.2 V input, as shown in Fig. 10(c). The proposed approach allows the DCO to ultimately operate at as low as 0.17 V of the harvested voltage.

To check for any spurs from the ring oscillator of non-overlapped clock generator, the measured phase noise with and without the DC-DC converter is shown in Fig. 10(d).



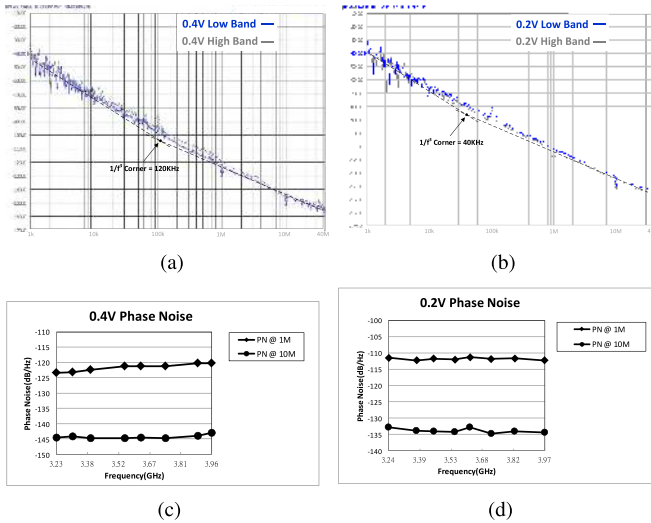


Fig. 9. Measured phase noise: (a) at 0.4 V; (b) at 0.2V; (c) at 0.4 V across tuning range; (d) at 0.2 V across tuning range.

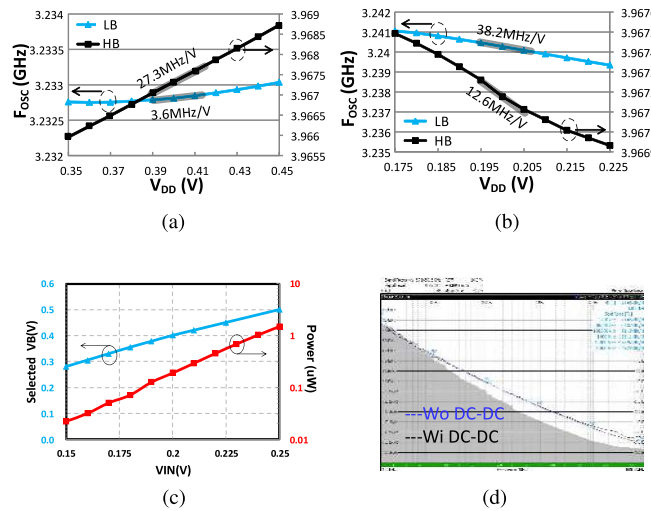


Fig. 10. Measurements of: (a) frequency pushing at 0.4 V; (b) frequency pushing at 0.2 V; (c) DC-DC converter; (d) phase noise spectrum wi/wo DC-DC converter.

TABLE I  
COMPARISON WITH STATE-OF-THE-ART ULV OSCILLATORS

	This Work		[10]	[11]	[12]	[13]
Technology	16nm FinFET	65nm	40nm	28nm	28nm	
VDD[V]	0.2 0.4	0.4	0.5	0.7	0.9	
Tuning Range[GHz]	3.2-4.0 (22%)	2.5-3.3 (27%)	3.3-4.5 (31%)	4.7-5.4 (14%)	2.9-3.8 (27%)	
Phase Noise [dBc/Hz] @ 10MHz	-134 -145	-147	-143	-138	-150	
Power [mW]	0.6 3.8	6.8	4.1	0.5	6.8	
FOM*	188 190	189	188	195	192	
Frequency Pushing(MHz/V)	12.6-38.2 3.6-27.3	180*	46-60	NA	NA	
1/f <sup>2</sup> Corner(KHz)	40 120	2000	60	200	200	
Core Area [mm <sup>2</sup> ]	0.11	0.15	0.1	0.18	0.19	

It exhibits no spurs, indicating the 3 kHz LPF is fulfilling its function. Table I shows comparison with state-of-the-art low-voltage LC-tank oscillators. Our  $V_{DD}$  is the lowest while delivering state-of-the-art performance. The area of 0.11 mm<sup>2</sup>

is among the lowest. The frequency pushing and flicker noise corner frequency are both the lowest, mainly due to the trifilar topology and the use of FinFET devices.

## VIII. CONCLUSION

This brief demonstrates a DCO for energy harvesting applications, which eliminates the intermediary power management system in conventional IoT solutions. By virtue of a trifilar-coil design, a passive voltage gain is boosted to overcome the start-up issues at a low supply voltage of 0.2 V. Separating the gate and drain voltages by the trifilar-coil transformer helps to bring the DCO supply below the threshold voltage. The variable capacitance from the gate side is separated from the main supply, thus eliminating the supply pushing effects by means of a low-pass filter. Fine tune resolution is achieved by means of impedance transformation from the tertiary coil. Class-F operation makes the waveform sharper for a better 1/f noise immunity and ISF. A tiny built-in DC-to-DC converter provides the gate biasing and control voltage for the switch capacitors with negligible power consumption. To operate at a low-supply voltage, a ring-based non-overlapped clock is generated by the gated inverters. Realized in TSMC 16-nm FinFET, it consumes sub-mW at 0.2 V, while achieving state-of-the-art performance. This brief shows a high potential for the solution of low-supply, low power consumption and low supply pushing in portable wireless applications.

## REFERENCES

- [1] Q. Wan, Y.-K. Teh, Y. Gao, and P.-K.-T. Mok, "Analysis and design of a thermoelectric energy harvesting system With reconfigurable array of thermoelectric generators for IoT application," *IEEE Trans. Circuits Syst. I, Reg. Papers*, vol. 64, no. 9, pp. 2346–2358, Sep. 2017.
- [2] C.-C. Li, M.-S. Yuan, C.-C. Liao, Y.-T. Lin, C.-H. Chang, and R. B. Staszewski, "All-digital PLL for Bluetooth low energy using 32.768-kHz reference clock and  $-0.45$ -V supply," *IEEE J. Solid-State Circuits*, vol. 53, no. 12, pp. 3660–3671, Oct. 2018.
- [3] F.-W. Kuo *et al.*, "An all-digital PLL for cellular mobile phones in 28 nm CMOS with  $-55$  dBc fractional and  $-91$  dBc reference spur," *IEEE Trans. Circuits Syst. I, Reg. Papers*, vol. 65, no. 11, pp. 3756–3768, Nov. 2018.
- [4] K. Kwok and H. C. Luong "Ultra-low-voltage high-performance CMOS VCOs using transformer feedback," *IEEE J. Solid-State Circuits*, vol. 40, no. 3, pp. 652–660, Mar. 2005.
- [5] M. Babaie and R. B. Staszewski, "Class-F oscillator," *IEEE J. Solid-State Circuits*, vol. 48, no. 12, pp. 3120–3133, Dec. 2013.
- [6] D. Park and S.-H. Cho, "Design techniques for a low-voltage VCO with wide tuning range and low sensitivity to environmental variations," *IEEE Trans. Microw. Theory Techn.*, vol. 57, no. 4, pp. 767–774, Apr. 2009.
- [7] C.-C. Li *et al.*, "A 0.2V trifilar-coil DCO with DC-DC converter in 16nm FinFET CMOS with 188dB FOM, 1.3kHz resolution, and frequency pushing of 38MHz/V for energy harvesting applications," in *Proc. IEEE Solid-State Circuits Conf.*, Feb. 2017, pp. 332–333.
- [8] S.-P. Hsu, "Problems in analysis and design of switching regulator," Ph.D. dissertation, Dept. Eng. Appl. Sci., California Inst. Technol., Pasadena, CA, USA, Sep. 1979.
- [9] Z. Luo, G. Wang, K. Yousef, B. Lau, Y. Lian, and C.-H. Heng, "A 0.0129 mm<sup>2</sup> DPLL with 1.6–2.0 ps RMS period jitter and 0.25-to-2.7 GHz tunable DCO frequency range in 55-nm CMOS," *IEEE Trans. Circuits Syst. II, Exp. Briefs*, vol. 65, no. 12, pp. 1844–1848, Dec. 2018.
- [10] L. Fanori and P. Andreani, "A 2.5-to-3.3GHz CMOS class-D VCO," *IEEE Int. Solid-State Circuits Conf. Dig. Tech. Papers*, Feb. 2013, pp. 332–333.
- [11] M. Shahmohammadi, M. Babaie, and R.-B. Staszewski, "A 1/f noise upconversion reduction technique applied to Class-D and Class-F oscillators," in *Proc. IEEE Solid-State Circuits Conf.*, Feb. 2015, pp. 444–445.
- [12] D. Murphy and H. Darabi, "A complementary VCO for IoE that achieves a 195dBc/Hz FOM and flicker noise corner of 200kHz," in *Proc. IEEE Solid-State Circuits Conf.*, Feb. 2016, pp. 44–45.
- [13] D. Murphy, H. Darabi, and H. Wu, "A VCO with implicit common-mode resonance," in *IEEE Int. Solid-State Circuits Conf. Dig. Tech. Papers*, Feb. 2015, pp. 442–443.